

**WL-TR-97-3083**



**FEASIBILITY ASSESSMENT AND  
OPTIMIZATION STUDY OF SMART  
ACTUATION SYSTEMS FOR  
ENHANCED AIRCRAFT MANEUVER  
PERFORMANCE**

**K. APPA  
J. AUSMAN**

**NORTHROP GRUMMAN CORPORATION  
MILITARY AIRCRAFT SYSTEMS DIVISION  
ONE HORNET WAY  
EL SEGUNDO, CA 90250-3277**

**N. S. KHOT**

**FLIGHT DYNAMICS DIRECTORATE  
WRIGHT LABORATORY  
AIR FORCE MATERIEL COMMAND  
WRIGHT-PATTERSON AIR FORCE BASE, OH 45433-7562**

**JULY 1997**

**FINAL REPORT FOR JUNE 1996 TO JUNE 1997**

**Approved for public release; distribution unlimited**

**FLIGHT DYNAMICS DIRECTORATE  
WRIGHT LABORATORY  
AIR FORCE MATERIEL COMMAND  
WRIGHT-PATTERSON AIR FORCE BASE, OH 45433-7562**

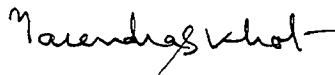
*19970912029*

## NOTICE

WHEN GOVERNMENT DRAWINGS, SPECIFICATIONS, OR OTHER DATA ARE USED FOR ANY PURPOSE OTHER THAN IN CONNECTION WITH A DEFINITE GOVERNMENT-RELATED PROCUREMENT, THE UNITED STATES GOVERNMENT INCURS NO RESPONSIBILITY OR ANY OBLIGATION WHATSOEVER. THE FACT THAT THE GOVERNMENT MAY HAVE FORMULATED OR IN ANY WAY SUPPLIED THE SAID DRAWING, SPECIFICATIONS, OR OTHER DATA, IS NOT TO BE REGARDED BY IMPLICATION, OR OTHERWISE IN ANY MANNER CONSTRUED, AS LICENSING THE HOLDER, OR ANY OTHER PERSON OR CORPORATION; OR AS CONVEYING ANY RIGHTS OR PERMISSION TO MANUFACTURE, USE, OR SELL ANY PATENTED INVENTION THAT MAY IN ANY WAY BE RELATED THERETO.

THIS REPORT IS RELEASEABLE TO THE NATIONAL TECHNICAL INFORMATION SERVICE (NTIS). AT NTIS, IT WILL BE AVAILABLE TO THE GENERAL PUBLIC, INCLUDING FOREIGN NATION.

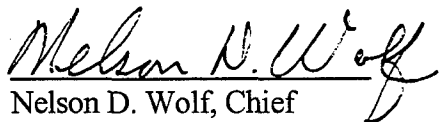
THIS TECHNICAL REPORT HAS BEEN REVIEWED AND IS APPROVED FOR PUBLICATION.



Narendra S. Khot  
Project Engineer  
Design and Analysis Branch



Mark Hopkins, Principal Engineer  
Vibration and Aeroelasticity Branch



Nelson D. Wolf, Chief  
Design and Analysis Branch  
Structures Division

IF YOUR ADDRESS HAS CHANGED, IF YOU WISH TO BE REMOVED FROM OUR MAILING LIST, OR IF THE ADDRESSEE IS NO LONGER EMPLOYED BY YOUR ORGANIZATION, PLEASE NOTIFY WL/FIBD BLDG 45, 2130 EIGHTH STREET, SUITE 1,



DEPARTMENT OF THE AIR FORCE

WRIGHT LABORATORY (AFMC)  
WRIGHT-PATTERSON AIR FORCE BASE, OHIO

14 OCT 97

FROM: WL/FIBD

SUBJECT: Errata to WL-TR-97-3083 titled, "Feasibility Assessment and Optimization Study of Smart Actuation Systems for Enhanced Aircraft Maneuver Performance."

The unedited copy of the subject technical report was inadvertently distributed in Aug 1997. If you have received the copy of this TR previously please discard it.

A handwritten signature in cursive script, appearing to read "Narendra S. Khot".

NARENDRA S. KHOT  
Research Aerospace Engineer  
Design & Analysis Branch  
Structures Division

19970912029

A329138

# REPORT DOCUMENTATION PAGE

Form Approved  
OMB No. 0704-0188

Public reporting burden for this collection of information is estimated to average 1 hour per response, including the time for reviewing instructions, searching existing data sources, gathering and maintaining the data needed, and completing and reviewing the collection of information. Send comments regarding this burden estimate or any other aspect of this collection of information, including suggestions for reducing this burden, to Washington Headquarters Services, Directorate for Information Operations and Reports, 1215 Jefferson Davis Highway, Suite 1204, Arlington, VA 22202-4302, and to the Office of Management and Budget, Paperwork Reduction Project (0704-0188), Washington, DC 20503.

<b>1. AGENCY USE ONLY (Leave blank)</b>		<b>2. REPORT DATE</b> 14 July 1997	<b>3. REPORT TYPE AND DATES COVERED</b> Final, 6-16-96 to 6-30-97.	
<b>4. TITLE AND SUBTITLE</b> Feasibility Assessment and Optimization Study of Smart Actuation Systems for Enhanced Aircraft Maneuver Performance			<b>5. FUNDING NUMBERS</b> C F33615-95-D-3215 PE 622401 PR 2401 TA 55 WU 00	
<b>6. AUTHOR(S)</b> K. Appa, J. Ausman, and N.S. Khot				
<b>7. PERFORMING ORGANIZATION NAME(S) AND ADDRESS(ES)</b> Northrop Grumman Corporation One Hornet Way El Segundo, California 90245-2804			<b>8. PERFORMING ORGANIZATION REPORT NUMBER</b>	
<b>9. SPONSORING / MONITORING AGENCY NAME(S) AND ADDRESS(ES)</b> FLIGHT DYNAMICS DIRECTORATE WRIGHT LABORATORY AIR FORCE MATERIEL COMMAND WRIGHT-PATTERSON AIR FORCE BASE, OHIO 45433-7562 POC: N. S. Khot, 937-255-6992			<b>10. SPONSORING / MONITORING AGENCY REPORT NUMBER</b>  WL-TR-97-3083	
<b>11. SUPPLEMENTARY NOTES</b>				
<b>12a. DISTRIBUTION / AVAILABILITY STATEMENT</b> Approved for Public Release; Distribution Unlimited			<b>12b. DISTRIBUTION CODE</b>	
<b>13. ABSTRACT (Maximum 200 words)</b> This report presents an analytical method developed to assess the power requirement and placement of the solid state actuators for enhanced maneuver performance of tactical fighters. Optimal control methodology is employed to compute the input stimuli such that the total power requirement is minimum with reduced peak stress levels. The study suggests that solid state actuators require some form of mechanical magnification of displacement for reduced control actuation power.				
<b>14. SUBJECT TERMS</b> Smart Actuation System, Feasibility Study, Optimal Control, Aircraft Maneuver			<b>15. NUMBER OF PAGES</b> 26	
			<b>16. PRICE CODE</b>	
<b>17. SECURITY CLASSIFICATION OF REPORT</b> Unclassified	<b>18. SECURITY CLASSIFICATION OF THIS PAGE</b> Unclassified	<b>19. SECURITY CLASSIFICATION OF ABSTRACT</b> Unclassified	<b>20. LIMITATION OF ABSTRACT</b> SAR	

## TABLE OF CONTENTS

<b>1 INTRODUCTION</b>	<b>1</b>
1.1 SUMMARY.....	1
1.2 TECHNICAL BACKGROUND.....	1
<b>2 ANALYTICAL MODELING OF SOLID STATE ACTUATION SYSTEM</b>	<b>7</b>
2.1 OVERVIEW.....	7
2.2 STEADY ROLL MANUEVER.....	7
2.3 OPTIMAL CONTROL DESIGN.....	9
2.4 HAMILTON EQUATIONS OF MOTION.....	10
2.5 SOLID STATE ACTUATOR ELEMENT FORMULATION.....	11
2.6 SOLID STATE ACTUATOR ENERGY.....	12
<b>3 IMPLEMENTATION OF THE DAMAGE TOLERANCE MODULE</b>	<b>13</b>
3.1 OUTLINE OF THE ALGORITHM.....	13
3.2 USER'S GUIDE.....	16
3.3 PROGRAMMER'S GUIDE.....	19
<b>4 DISCUSSION OF RESULTS</b>	<b>25</b>
4.1 TESTS MODEL.....	25
4.2 TEST CASE: STEADY ROLL MANEUVER.....	26
<b>5 CONCLUSIONS AND RECOMMENDATIONS</b>	<b>31</b>
<b>REFERENCES</b>	<b>32</b>

## PREFACE

This report describes the work performed by advanced structural methods department of Northrop Grumman Corporation, Military Aircraft Systems Division, for the Flight Dynamics Directorate, Wright Laboratory, Air Force Material Command, Wright Patterson Air Force Base, Ohio, under contract F33615-95-D-3215, Project No. 0003, "Feasibility Assessment and Optimization Study of Smart Actuation Systems for Enhanced Aircraft Maneuver Performance."

The final report describes the theoretical development of the optimal control methodology applied to determine solid state actuator placement and forces required to perform steady rolling maneuver of flexible aircraft at desired roll rate. This algorithm is used employing ASTROS generated data base. A few test cases showing actuator power requirement are demonstrated.

Dr. Narendra S. Khot, Structures Division, Flight Dynamics Directorate, Wright Laboratory, initiated the solid state actuator feasibility study program and also served as the technical monitor. Dr. Kari Appa was the principal investigator. Mr. John Ausman was responsible for implementing the optimal control algorithm in conjunction with the ASTROS module to generate the required data.

# 1. INTRODUCTION

## 1.1 Summary

The performance characteristics of aircraft largely depend on the quality and distribution of air flow on the lifting surfaces. By nature, birds are able to configure their wings in such a manner that the air flow quality and flying efficiency are at optimum conditions. Duplication of such air flow characteristics on manufactured flying vehicles has been a desired objective of airplane designers, beginning with the Wright brothers. To simulate bird-like flying characteristics, the lifting surfaces must be able to deform smoothly at appropriate locations. In the mid 1980s, the Air Force sponsored a mission adaptive wing (MAW) project to study aerodynamic and maneuver performance characteristics of tactical aircraft (Refs. 1, 2 and 3). An F-111 aircraft was selected and fitted with hydraulic actuators to deform the wing. This aircraft was test flown in several mission performances. The test results showed overwhelming aerodynamic performance benefits and agility characteristics. However, the actuation system was heavy and expensive to operate, so practical implementation of this concept could not be realized at that time.

Recent analytical and wind tunnel studies sponsored by ARPA and the Air Force (Ref. 4) show how smoothly contoured control surfaces promote incremental growth in suction pressure near the leading edge. This has a beneficial effect on control surface effectiveness, leading to enhanced aircraft maneuver performance. A few test cases taken from this study are presented in the next section to emphasize the need for active control of lifting surface camber to enhance aircraft performance. This report, in subsequent sections, describes an analytical approach which can be used to determine optimum wing camber and also to command the solid state actuators to deform the desired lifting surface to match this optimal shape.

## 1.2 Technical Background

In conventional aircraft, the leading and trailing edge control surfaces are used as aerodynamic effectors to generate desired lift distributions on wings and control surfaces. The leading edges are generally used to minimize flow separation at moderately high angle of attack flight maneuver cases, while the trailing edges are used to obtain desired pitching and rolling moments.

Two factors limit the effectiveness of the trailing edge control surfaces. First, the control effectiveness decreases with increasing dynamic pressure due to

aeroelastic effects (i.e. adverse twisting of the wing). The second problem is that there exists a massive flow separation along the hinge line, resulting in reduced aerodynamic loading on the wing as well as on the control surface. Figure 1-1a shows flow separation results from a rapid change in control surface slope at the hinge line. This problem can be alleviated by the use of hingeless contoured trailing edges as shown in Figure 1-1b and Figure 1-1c.

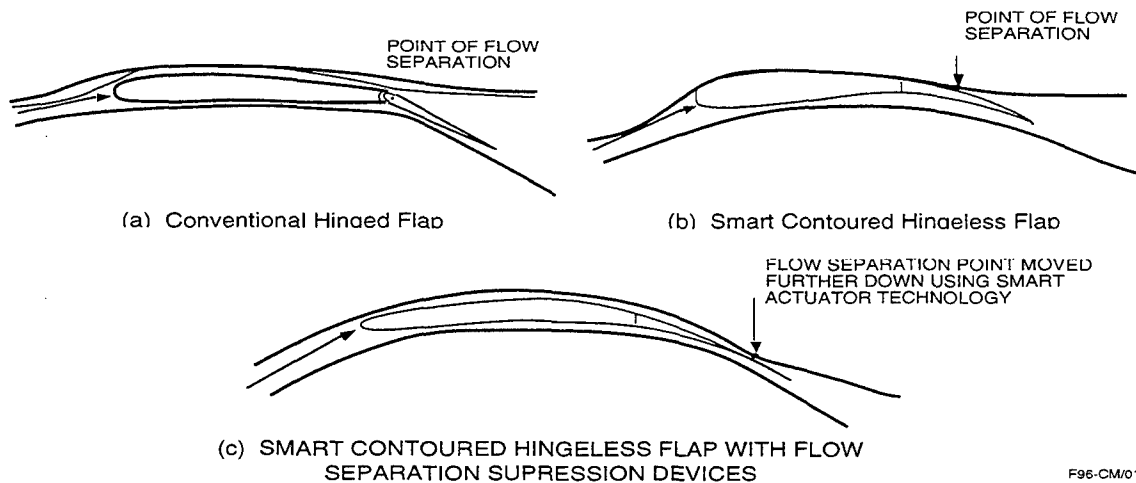


**Figure 1-1. Flow Characteristics Over Hinged and Hingeless Contoured Control Surfaces**

A flow separation suppression device can be used to move the point of separation towards the trailing edge. Use of such devices will be investigated at a later time. To demonstrate the difference in pressure distributions between hinged flap and smoothly contoured flaps, a few studies using a computational fluid dynamics (CFD) method were conducted. Subsequently, wind tunnel tests were also conducted at NASA Langley in their Transonic Dynamic Tunnel (TDT) under the DARPA/WL "Smart Materials and Structures - Smart Wing" contract (F33615-93-C-3202).

The CFD solutions are shown in Figure 1-2, in which the solid curve represents the pressure distribution computed for contoured trailing edge surface, while the dotted curve denotes the data obtained using a hinged flap. The hinged flap data depict flow separation at the trailing edge, whereas the contoured flap shows large suction pressure on the flap, as well as on most of the upper surface. This type of pressure distribution has some beneficial effects on aeroelastic stability. Since the elastic axis lies downstream of the section aerodynamic center, the increased load near the leading edge twists the wing upwards, resulting in an increased angle of attack relative to that observed in the case of a conventional trailing edge flap. Thus, the effectiveness of the trailing edge control surface increases with increased



dynamic pressure, and consequently, the roll reversal speed increases. This is a significant contrast to the case of traditional control surfaces where the agility of the aircraft is reduced with increasing dynamic pressure.

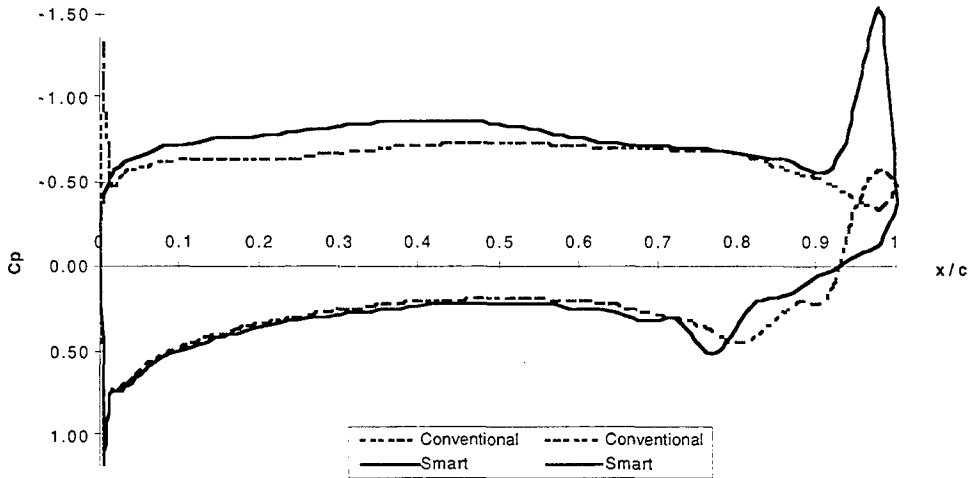


**Figure 1-2. Comparison of Pressure Distribution Between Hinged and Hingeless Contoured Control Surfaces**

In the case of wind tunnel tests, two models were constructed. One model had conventional hinged trailing edge flaps and ailerons, while the other (also known as the Smart Wing) had deformable control surfaces made of shape memory alloys (SMA). Typical wind tunnel results are presented in Figure 1-3 through Figure 1-5. The trends are similar to those observed in the CFD solutions. However, due to lack of instrumentation, the pressure loop for the hinged control surface was not observed in the wind tunnel data.

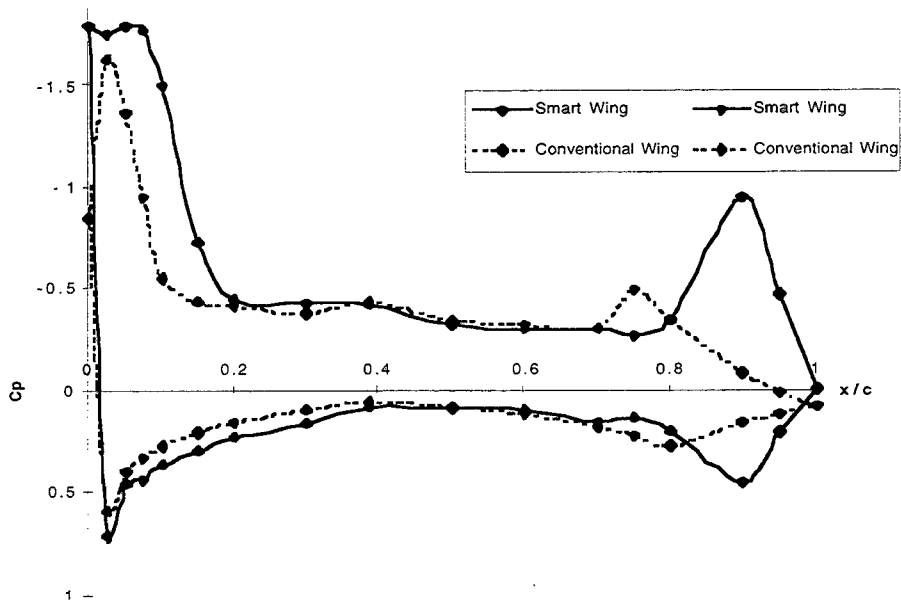


Figure 1-3. Pressure Coefficient ( $C_p$ ) Comparison, at 36% Span  
 $Q = 60$  psf,  $\alpha = 8^\circ$ , Flap =  $10^\circ$ , Aileron =  $0^\circ$  (Run 100 vs. 80)

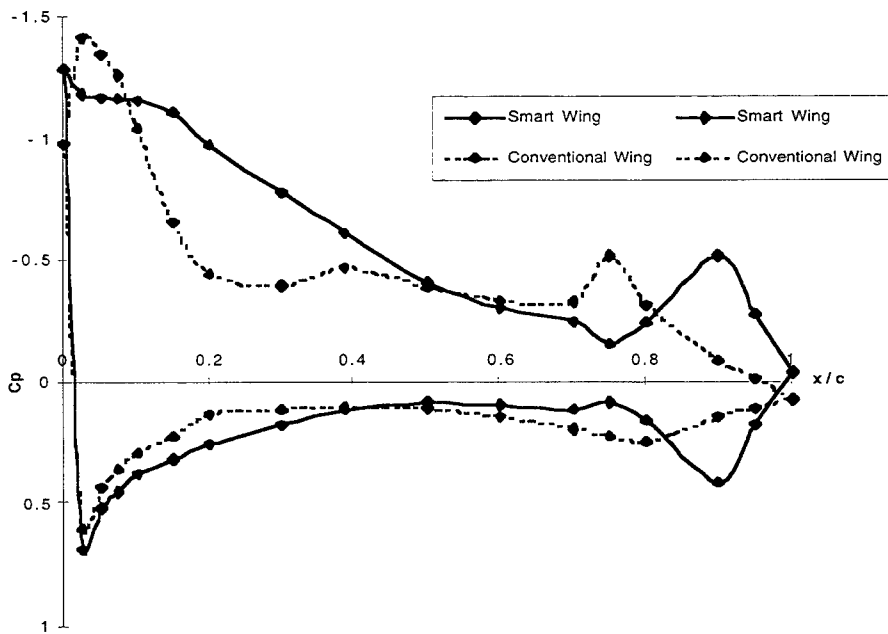


Figure 1-4. Pressure Coefficient ( $C_p$ ) Comparison, at 50% Span  
 $Q = 60$  psf,  $\alpha = 8^\circ$ , Flap =  $10^\circ$ , Aileron =  $0^\circ$  (Run 100 vs. 80)

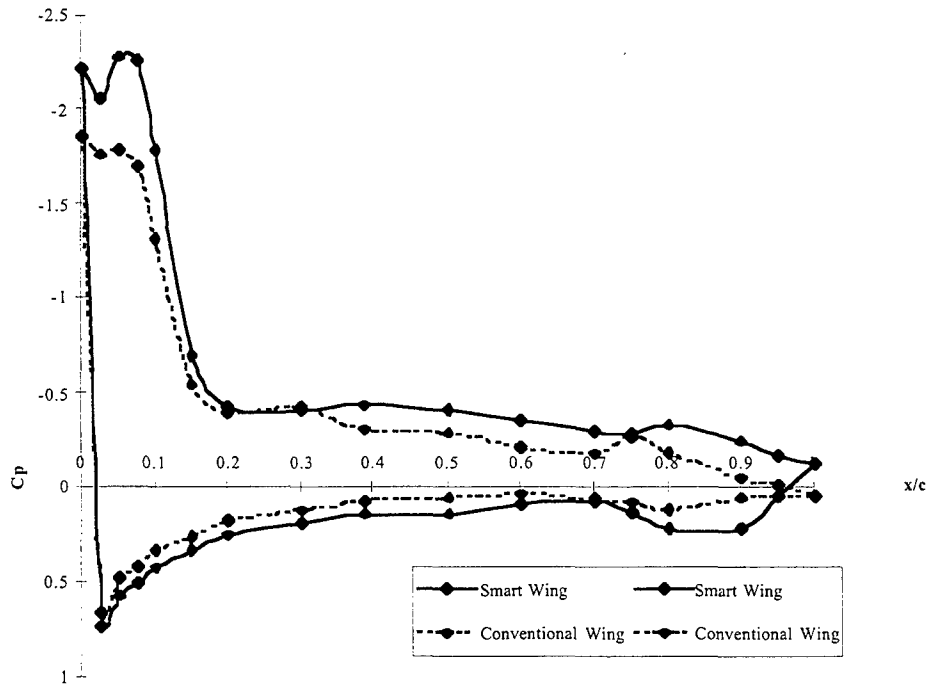
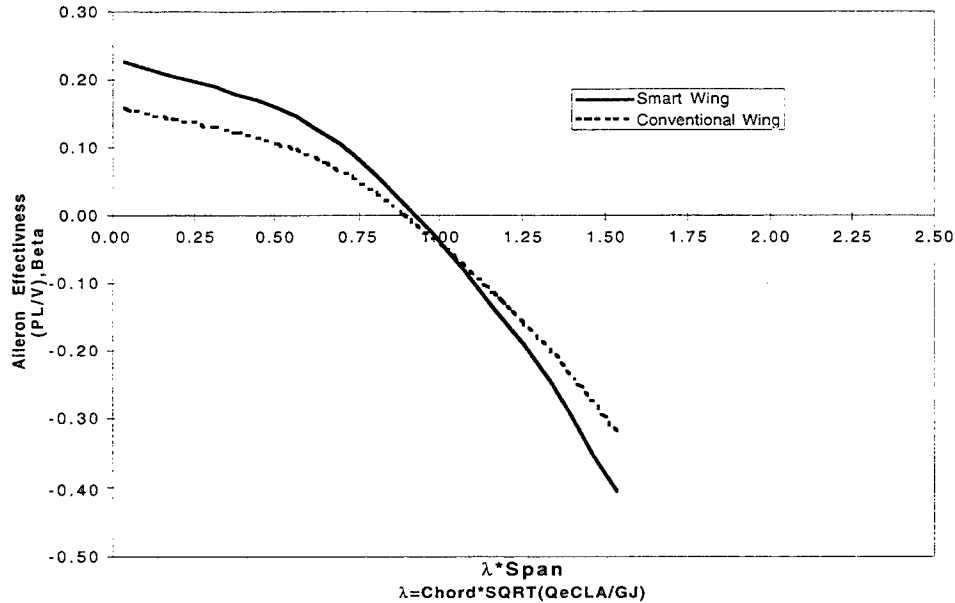


Figure 1-5. Pressure Coefficient ( $C_p$ ) Comparison, at 80% Span  
 $Q = 120$  psf,  $\alpha = 8^\circ$ , Flap =  $0^\circ$ , Aileron =  $0^\circ$  (Run 109 vs. 20)

Aerodynamic coefficients (both lift and rolling moment) due to aileron deflection were measured in the wind tunnel and were used to compute the roll reversal speed. These coefficients are shown in Figure 1-6. The roll reversal speed is the velocity at which the aileron effectiveness is equal to zero. As expected, the hingeless control surface yields a higher roll rate and a higher control reversal speed compared to the hinged control surface.



**Figure 1-6. Aileron effectiveness Vs. Nondimensional Dynamic Pressure**

Thus, hingeless control surfaces offer many improvements over traditional control surfaces. Chief among these improvements is the improved aerodynamic performance. Hence, there is a compelling reason to investigate various avenues, in the light of smart structures technology, to develop feasible mechanisms to control the camber of lifting surfaces, as is desired in any combat mission.

Today, with the advent of new materials technology, it is possible to design smoothly deforming lifting surfaces using composite materials. Also, solid state actuators, which can output large forces at rates used in modern flight control algorithms, are also being developed. These actuators can also be built in relatively small sizes and with light weight. Since these actuators are small and light, large number of these actuators can be used on the lifting surface so that any desired lifting surface deformation shape can be commanded for any given mission flight condition.

To operate these solid state actuators with minimum power, there is a need to determine appropriate actuator locations and power ratings of the individual actuators. This report discusses a mathematical approach based on optimal control theory. Aircraft performance goals, such as pitch, roll and yaw rates, are used as the target quantities (constraints), while actuator power rating is taken as the objective function of the design problem. Detailed discussions of the synergetic design methodology, including the balancing of the aircraft, are presented in References 5 through 8. A brief summary related to the solid state actuator is presented next.

## 2. ANALYTICAL MODELING OF SOLID STATE ACTUATION SYSTEM

### 2.1 Overview

The main objective of this study is to develop an analytical model which helps to select the actuator locations and power required for each actuator, so that desired aircraft angular rates (pitch, roll and yaw) can be achieved without weight penalty. A building block approach is used to develop the algorithm so that more complex maneuver performance requirements and structural design requirements can be added later.

### 2.2 Steady Roll Maneuver

To develop the mathematical basis of the solid state actuation system, a steady roll maneuver case is considered first. The equilibrium equations for this problem can be written as:

$$K \cdot r + Q \cdot T^T \cdot A \cdot \alpha + F \cdot u = 0 \quad (2-1)$$

where:

- $\alpha$  = Angle of attack at aerodynamic panels
- $A$  = Aerodynamic Influence Coefficients (AIC) matrix with respect to aerodynamic panels
- $F$  = Nodal forces generated from the actuator elements
- $K$  = Structural stiffness matrix in structural degrees of freedom (DOF)
- $r$  = Displacement vector
- $T$  = Transformation matrix from structural DOF to aerodynamic DOF
- $u$  = Vector of actuator stimuli (input)

The displacement vector,  $r$ , can be expressed as a linear combination of rigid body modes and vibration modes. Thus, we have:

$$r = [\psi_r, \psi_e] \begin{Bmatrix} \eta_r \\ \eta_e \end{Bmatrix} = [\psi] \eta \quad (2-2)$$

where:

- $\Psi_r$  = Vector of rigid body modes in rolling motion ( $\phi$ )
- $\Psi_e$  = Matrix of antisymmetric vibration modes
- $\eta$  = Vector of generalized coordinates,  $\{\eta_r, \eta_e\}$
- $\phi$  = Roll angle (radians)

The subscript 'r' denotes rigid body modes, while 'e' denotes the elastic vibration modes.

The angle of attack at the control points of the aerodynamic panels is given by:

$$\alpha = T \frac{\dot{r}}{V} = \frac{1}{V} T \left[ \frac{\partial r}{\partial t} + U \cdot \nabla r \right] = \frac{1}{V} T \left[ \Psi_r p + u \frac{\partial \Psi_e}{\partial x} \eta_e \right] \quad (2-3)$$

where:

- V = Free stream velocity
- T = Transformation matrix relating the deformation from structural points to aerodynamic points
- p = Roll rate,  $\dot{\phi}$
- u = Chordwise component of V

The velocity component due to  $\dot{\eta}_e$  is omitted because it is small in comparison to the rolling velocity, p.

Equation (2-1) can be rewritten in terms of generalized coordinates,  $\eta$ :

$$\bar{K} \begin{Bmatrix} p \\ \eta_e \end{Bmatrix} + QA \begin{Bmatrix} p \\ \eta_e \end{Bmatrix} + \mathfrak{S}u = 0 \quad (2-4)$$

in which the generalized stiffness is given by:

$$\bar{K} = \begin{bmatrix} 0 & 0 \\ 0 & k_{ee} \end{bmatrix} \quad (2-5)$$

This equation can be solved for p and  $\eta_e$ :

$$\begin{Bmatrix} p \\ \eta_e \end{Bmatrix} = -[\bar{K} + QA]^{-1} \mathfrak{S}u = \begin{bmatrix} B \\ C \end{bmatrix} u \quad (2-6)$$

Then the roll rate is given by:

$$p = Bu \quad (2-7)$$

and the generalized coordinates of the elastic modes are:

$$\eta_e = Cu \quad (2-8)$$

For a given distribution of actuator stimuli ( $u$ ), one can calculate the roll rate  $p$  from equation 2-7. However, for a specified roll rate, ( $p_{reqrd}$ ) the input stimuli,  $u$ , cannot be determined from equation 2-7. This problem will be solved using optimal control theory, discussed next.

### 2.3 Optimal Control Design

This problem can be solved by the method of optimal control theory. Hence, the Hamiltonian function can be stated as:

$$h = \frac{1}{2} \varepsilon^T Q \varepsilon + U(\xi) + \lambda^T (Ap + B\xi) \quad (2-9)$$

where:

- A = -1 from equation (2-7)
- $\varepsilon$  = Vector of target error function which must go to zero to satisfy all performance requirements
- Q = Weighting matrix
- $\lambda$  = Vector of Lagrangian coefficients

In the present problem, the target vector (error) is given by:

- a. Constraint on roll rate:

$$\varepsilon(1) = (1 - p/p_T) \quad (2-10)$$

where  $p_T$  is the required roll rate in the velocity range up to  $V_R$ .

- b. Constraint on strains in the actuator materials:

$$\varepsilon(1+j) = (1 - c_j u / \varepsilon_a) \quad (2-11)$$

where:

- $\epsilon_a$  = Allowable strain in the piezo electric material
- $c_j$  = Strain per unit of electrical input (volt) for actuator number j

The main objective of this constraint is to limit the power input so that the actuator is not overly strained beyond elastic limit. Likewise, stress or strain constraints on primary structural members may also be imposed.

The second term, U, in equation (2-9), is the objective function representing the control power. It may also include structural weight and aerodynamic figures of merit, which may be considered in the subsequent studies.

In the following discussion, the state variable X denotes the roll rate, p, and  $\xi$  represents the control variable, u (or the input stimuli).

The control power is the sum of work done by each actuator:

$$U(\xi) = \sum_l^m W_l = \frac{1}{2} \xi^T R \xi \quad (2-12)$$

where:

- $\xi$  = vector of control variables (u)
- R = weighting matrix

## 2.4 Hamiltonian Equations of Motion

Differentiating the Hamiltonian function, H (Equation 2-9), with respect to  $X(=p)$ ,  $\xi(=u)$ , and  $\lambda$ , and using the principle of optimal control theory, we obtain the following two-point boundary value problem:

$$\begin{Bmatrix} \dot{p} \\ \dot{\lambda} \end{Bmatrix} = \begin{bmatrix} h_{11} & h_{12} \\ h_{21} & h_{22} \end{bmatrix} \begin{Bmatrix} p \\ \lambda \end{Bmatrix} + \begin{Bmatrix} F_1 \\ F_2 \end{Bmatrix} = [H] \begin{Bmatrix} p \\ \lambda \end{Bmatrix} + \begin{Bmatrix} F_1 \\ F_2 \end{Bmatrix} \quad (2-13)$$

together with the incremental control (design) input:

$$\xi = -\mathfrak{R}^{-1} [B^T] \lambda \quad (2-14a)$$

in which

$$\mathfrak{R} = [R_i + (Q_{1+i} c_i / \epsilon_a)^2] \quad \text{is a diagonal matrix for } i=1, \dots, n \text{ actuators} \quad (2-14b)$$



The elements of the Hamiltonian matrix, H, in equation (2-13) are given by:

$$h_{11} = A \quad (2-15)$$

$$h_{12} = -B\mathfrak{R}^{-1}B^T \quad (2-16)$$

$$h_{21} = -Q/(p_T * p_T) \quad (2-17)$$

$$h_{22} = -h_{11}^T \quad (2-18)$$

$$F_1 = -B\mathfrak{R}^{-1} \left\{ \begin{array}{c} Q_{1+i}c_i \\ \varepsilon_a \end{array} \right\} \quad \text{for } i=1, \text{ n actuators} \quad (2-19)$$

$$F_2 = -Q/p_T \quad (2-20)$$

Since we are dealing with a steady rolling maneuver, the left hand side of equation (2-13) can be set to zero, and solved for p and  $\lambda$ . Thus, we obtain:

$$\begin{bmatrix} p \\ \lambda \end{bmatrix} = -[H]^{-1} \begin{bmatrix} F_1 \\ F_2 \end{bmatrix} \quad (2-21)$$

The actuator input for required roll rate ( $p_T$ ) is given by:

$$\xi(=u) = -\mathfrak{R}^{-1}[B^T]\lambda \quad (2-14a)$$

## 2.5 Solid State Actuator Element Formulation

The actuators can be represented as rod elements, consisting of usual element degrees of freedom and additional degrees of freedom to represent input stimuli either in the form of an electric field or a magnetic field.

Consider the 6x1 strain vector given by:

$$\varepsilon = \varepsilon_e + \varepsilon_{em} \quad (2-22)$$

where:

$$\varepsilon_e = \text{Strain due to elastic deformation}$$

$$\varepsilon_{em} = \text{Strain due to electric field}$$

$\varepsilon_{em}$  can be defined as:

$$\varepsilon_{em} = D \cdot u \quad (2-23)$$

where:

$$\begin{aligned} u &= 3 \times 1 \text{ vector of electric field, } e \text{ (volt/meter)} \\ D &= 6 \times 3 \text{ displacement matrix (meter/volt)} \end{aligned}$$

Then, the strain energy is given by:

$$U = \frac{1}{2} \iiint \epsilon^T E \epsilon dV \quad (2-24)$$

From the variational principal, the element matrices can be written as:

$$\begin{bmatrix} K_{rr} & K_{ru} \\ K_{ur} & K_{uu} \end{bmatrix} \begin{Bmatrix} r \\ u \end{Bmatrix} = \begin{Bmatrix} \text{actuator} \\ \text{sensor} \end{Bmatrix} \quad (2-25)$$

The first set of equations represents the function of the actuator in which a force vector is generated due to external stimuli,  $u$ . The second set of equations denote the function of a sensor, wherein the elements put out electrical signals due to the deformation of the structure. The stiffness matrix  $K_{rr}$  is computed in ASTROS, while the load matrix  $K_{ru}$  is computed in the new module and assembled into the actuator force matrix,  $F$ , as denoted in equation (2-1).

## 2.6 Solid State Actuator Energy

Consider a piezoceramic actuator. The energy in the element under impressed electric field is given by:

$$W = \frac{1}{2} \epsilon_0 e^T e (\text{Vol}) \quad (2-26)$$

where:

$$\begin{aligned} \epsilon_0 &= \text{Permittivity of the material (Coulomb}^2/\text{Newton} \cdot \text{Meter}^2) \\ e &= \text{Electric field} \end{aligned}$$

# 3. COMPUTER PROGRAM IMPLEMENTATION WITH ASTROS

## 3.1 Outline of the Algorithm

The current implementation of the Smart Actuation system is a two step process, illustrated in Figure 3-1.

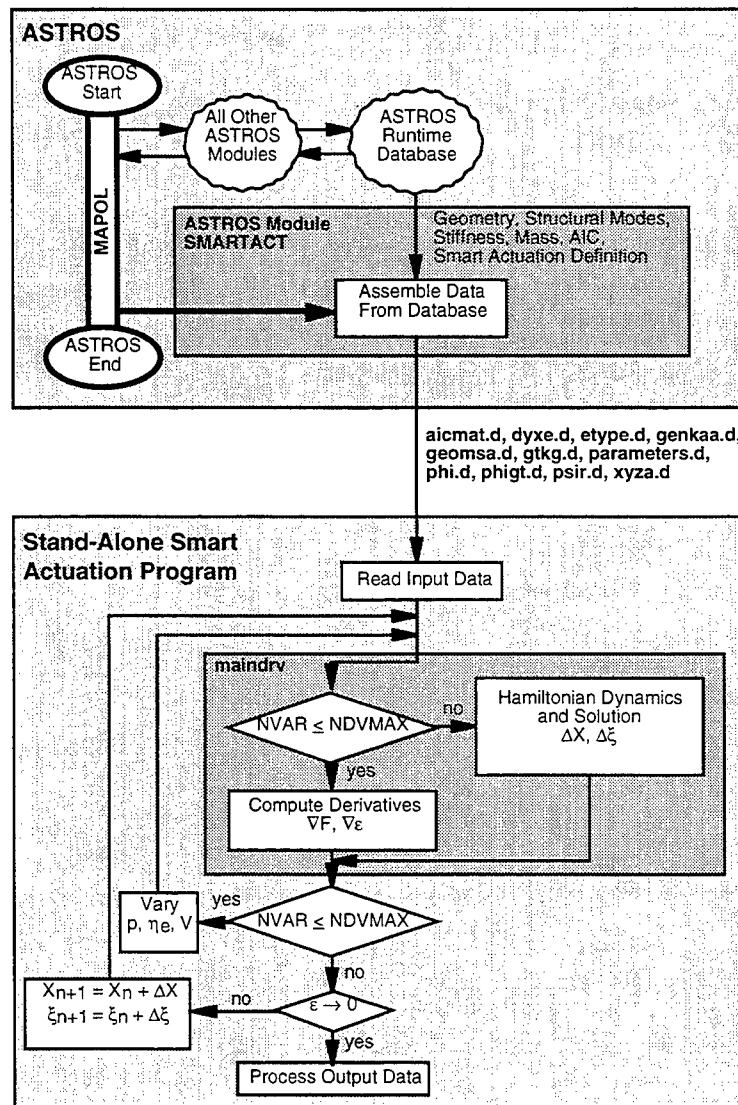


Figure 3-1. Overview of ASTROS/Smart Actuation System

### 3.1.1 Step One

In the first step, a special version of ASTROS is run. This version of ASTROS will process the data that is required for Smart Actuation program. Two additional bulk data entries, **SACNTL** and **SAELIST**, are required to define data that is specific to this process. These bulk data entries are described in subsequent sections. The following files are generated by ASTROS:

	Format	Description
aicmat.d	1000(1X,E12.5)	Matrix of aerodynamic influence coefficients.
dyxe.d	1000(1X,E12.5)	$\frac{\partial \psi_e}{\partial x}$ Transforms elastic modes to aerodynamic panels.
etype.d	A8	Element types
genkaa.d	1000(1X,E12.5)	Generalized stiffness matrix.
geomsa.d	2(I8,1X),3(1PE12.5,1X)	Steady aerodynamics geometry description: <u>Column</u> <u>Description</u> 1   External aerodynamic box ID 2   Internal aerodynamic box ID 3   X location of box centroid in basic coordinates 4   Y location of box centroid in basic coordinates 5   Z location of box centroid in basic coordinates
gtk.d	1000(1X,E12.5)	ASTROS [GTKG] matrix.
parameters.d	FORTTRAN 'Parameter'	Problem-dependent variable values which should be included in Kari Appa's Smart Actuation program.
phi.d	1000(1X,E12.5)	Matrix of mode shapes.
phigt.d	1000(1X,E12.5)	Transpose of ASTROS [PHIG] matrix.
psir.d	1000(1X,E12.5)	Rigid body modes matrix.
xyza.d	I8,14(1PE12.5)	Actuator element descriptions:

<u>Column</u>	<u>Description</u>
1	Element ID
2	X Coordinate of grid 1 in the basic system
3	Y Coordinate of grid 1 in the basic system
4	Z Coordinate of grid 1 in the basic system
5	X Coordinate of grid 2 in the basic system
6	Y Coordinate of grid 2 in the basic system
7	Z Coordinate of grid 2 in the basic system
8	X Coordinate of grid 3 in the basic system
9	Y Coordinate of grid 3 in the basic system
10	Z Coordinate of grid 3 in the basic system
11	X Coordinate of grid 4 in the basic system
12	Y Coordinate of grid 4 in the basic system
13	Z Coordinate of grid 4 in the basic system
14	Young's Modulus
15	Cross sectional area or membrane thickness

### 3.1.2 Step Two

The second step of the process is to run the Smart Actuation program. The data sets that were generated in Step One are used as inputs to the Smart Actuation program.

## 3.2 User's Guide

### 3.2.1 Overview

This section provides updates to the ASTROS User's Manual. The sections that are affected are noted where appropriate.

### 3.2.2 MAPOL Engineering Modules

This section provides additional documentation to Section 2.4.2.1 of the ASTROS User's Manual.

MODULE	TYPE	DESCRIPTION
SMARTACT	ENGINEERING	Compute and assemble data required for Smart Actuation calculations.

### 3.2.3 Bulk Data Descriptions

This section provides additional documentation to Section 4.7 of the ASTROS User's Manual.

## Input Data Entry SACNTL

Description: Defines control parameters to the Smart Actuation module.

### Format and Example:

1	2	3	4	5	6	7	8	9	10
SACNTL	SID	ITRMAX	RMODES	EMODES	ERRTOL				

SACNTL	101	10	1	3	0.001				
--------	-----	----	---	---	-------	--	--	--	--

Field	Contents
-------	----------

- SID** Set identification number (Integer > 0)
- ITRMAX** Maximum number of design iterations (Integer > 0)
- RMODES** Set identification number of a **MODELIST** bulk data entry that is used to request the rigid body modes that are to be used for the Smart Actuation analysis (Integer)
- EMODES** Set identification number of a **MODELIST** bulk data entry that is used to request the elastic modes that are to be used for the Smart Actuation analysis (Integer)
- ERRTOL** Iteration convergence criteria (Real, Default = 0.001)

**Input Data Entry SAELIST**

**Description:** Defines the list of actuation elements to the Smart Actuation module.

**Format and Example:**

1	2	3	4	5	6	7	8	9	10
SAELIST	SID	ETYPE	EID1	EID2	EID3	EID4	EID5	EID6	CONT
CONT	EID7	EID8	-etc-						

SAELIST	1001	ROD	1001	1002	1003	1004			
---------	------	-----	------	------	------	------	--	--	--

**Alternate Form:**

1	2	3	4	5	6	7	8	9	10
SAELIST	SID	ETYPE	EID1	THRU	EID2				

Field	Contents								
<b>SID</b>	Set identification number. (Integer > 0)								
<b>ETYPE</b>	Character input identifying the element type (See Note 1). One of the following:  <table border="0" style="margin-left: 100px;"> <tr> <td>BAR</td><td>SHEAR</td></tr> <tr> <td>QDMEM1</td><td>TRIA3</td></tr> <tr> <td>QUAD4</td><td>TRMEM</td></tr> <tr> <td>ROD</td><td></td></tr> </table>	BAR	SHEAR	QDMEM1	TRIA3	QUAD4	TRMEM	ROD	
BAR	SHEAR								
QDMEM1	TRIA3								
QUAD4	TRMEM								
ROD									
<b>EID<sub>i</sub></b>	Element identification number (Integer > 0 or blank)								

**Remarks:**

1. Currently, only the **ROD** element is supported by the Smart Actuation algorithm. All other element types are included here for future development.
2. **SID** is here for future implementations of the Smart Actuation system which may be more general.
3. If the alternate form is used, **EID2** must be greater than or equal to **EID1**.
4. Nonexistent elements may be referenced and will result in no error message.
5. Any number of continuations is allowed.



## **3.3 Programmer's Guide**

### **3.3.1 Overview**

This section provides updates to the ASTROS Programmer's Manual. The sections that are affected are noted where appropriate.

### **3.3.2 Engineering Application Modules**

This section provides additional documentation to Section 5 of the ASTROS Programmer's Manual.

# Engineering Application Module: SMARTACT

Entry Point: SMARTACT

Purpose:

To assemble and calculate data required for Smart Actuation analysis

MAPOL Calling Sequence:

```
CALL SMARTACT ( BC, SACNTL, SAELIST, [PHIG(BC)], LAMBDA,  
BGPDT(BC), BEAMEST, QDMM1EST, QUAD4EST,  
RODEST, SHEAREST, TRIA3EST, TRMEMEST,  
[DYX], [GENKAA], [GENMAA],  
AAICMAT(MINDEX)], TRIM, OGPWG, CASE,  
GEOMSA, [GTKG], MAT1, MODELIST);
```

BC	Boundary condition number(Integer, Input)
SACNTL	Relation of smart actuation control parameters (Input)
SAELIST	Relation of smart actuation elements (Input)
[PHIG(BC)]	Matrix of global eigenvectors from real eigenanalysis (Input)
LAMBDA	Relation of real eigenvalue analysis results (Input)
BGPDT(BC)	Basic grid point definition table (Input)
BEAMEST	Relation summarizing the C <sub>BAR</sub> element (input)
QDMM1EST	Relation summarizing the C <sub>QDMM1</sub> element (input)
QUAD4EST	Relation summarizing the C <sub>QUAD4</sub> element (input)
RODEST	Relation summarizing the C <sub>ONROD</sub> and C <sub>ROD</sub> element (input)
SHEAREST	Relation summarizing the C <sub>SHEAR</sub> element (input)
TRIA3EST	Relation summarizing the C <sub>TRIA3</sub> element (input)
TRMEMEST	Relation summarizing the C <sub>TRMEM</sub> element (input)

<b>[DYX]</b>	Elastic modes splined to the aerodynamic model (input)
<b>[GENKAA]</b>	Generalized stiffness (Input)
<b>[GENMAA]</b>	Generalized mass (Input)
<b>[AAICMAT (MINDEX) ]</b>	Antisymmetric aerodynamic influence coefficients (Input)
<b>TRIM</b>	Relation containing trim parameters (Input)
<b>OGPWG</b>	Relation containing data from the grid point weight generation computations (Input)
<b>CASE</b>	Relation containing the case parameters for each analysis within each boundary condition (Input)
<b>GEOMSA</b>	Relation containing data on the geometric location of the aerodynamic degrees of freedom (Input)
<b>[GTKG]</b>	Interpolation matrix relating the forces at the aerodynamic degrees of freedom to the forces at the global structural degree of freedom (Input)
<b>MAT1</b>	Relation containing material properties (Input)
<b>MODELIST</b>	Relation containing lists of normal modes

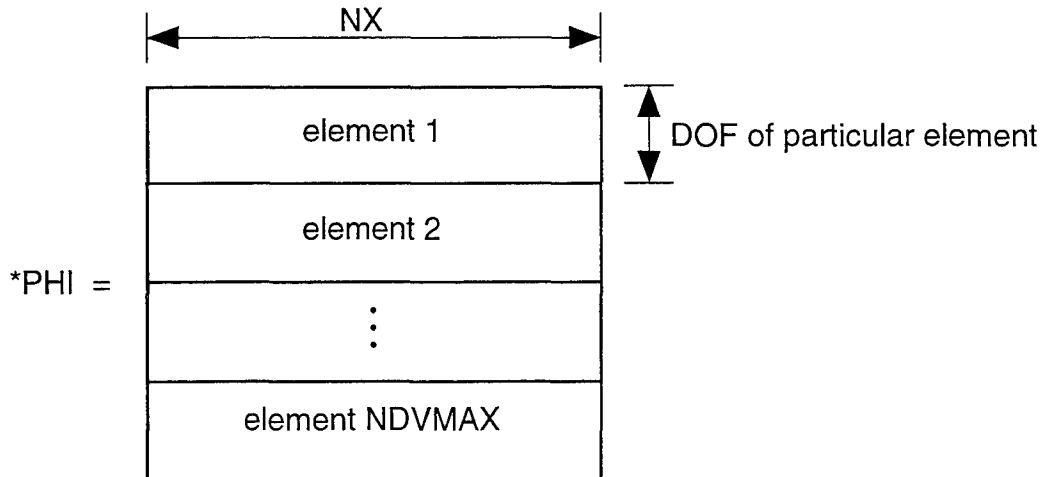
Application Calling Sequence:

None

Method:

First the **CASE** entries associated with **SAERO** and **SAERO2** subcases for the current boundary condition are read into memory. The number of normal modes is obtained by opening the **[PHIG]** matrix. The lists of normal modes are read from the **MODELIST** entries. The control parameters from the **SACNTL** entries are then read. Then the list of smart actuation elements is read from the **SAELIST** entries. The material properties are read from the **MAT1** entries. The Basic Grid Point Definition Table is read from the **BGPDT** relation. For each smart actuation element, the data in the associated **\*EST** relation is read. The G-Set modes matrix is read and transposed. The **DYX** matrix is read and reduced to the number of elastic

modes. The **GTKG** interpolation matrix is read. The **PHI** matrix and **XYZA** matrices are assembled for the smart actuation elements. **PHI** describes, for each mode, the generalized behavior for each smart actuation element and has the following form:



The **XYZA** matrix describes the smart actuation element connectivity. The generalized mass and stiffness matrices are read. The **AIC** matrix is read. The free stream velocity is read from the **TRIM** relation. The center of gravity is read from the **OGPWG** relation. The aerodynamic geometry is read in from the **GEOMSA** relation. **PSIR**, the rigid body aerodynamic modes matrix, is assembled. The data required for the smart actuation loop is now assembled.

Design Requirements:

None

Error Conditions:

None

### 3.3.3 Database Entity Descriptions

This section provides additional documentation to Section 9 of the ASTROS Programmer's Manual.

Entity: **SACNTL**

Entity Type: Relation

Description: Contains control parameters for the Smart Actuation System.

Relation

Attributes:

<b>NAME</b>	<b>TYPE/KEY</b>	<b>DESCRIPTION</b>
<b>SID</b>	Integer > 0	Set identification number
<b>ITRMAX</b>	Integer > 0	Maximum number of design iterations
<b>RMODES</b>	Integer	Set identification number of a <b>MODELIST</b> bulk data entry that is used to request the rigid body modes that are to be used for the Smart Actuation analysis
<b>EMODES</b>	Integer	Set identification number of a <b>MODELIST</b> bulk data entry that is used to request the elastic modes that are to be used for the Smart Actuation analysis
<b>ERRTOL</b>	REAL	Iteration convergence criteria

Created By: Module IFP

Entity: **SAELIST**  
 Entity Type: Relation  
 Description: Contains the list of smart actuation elements.  
 Relation  
 Attributes:

<b>NAME</b>	<b>TYPE/KEY</b>	<b>DESCRIPTION</b>
<b>SID</b>	Integer > 0	Set identification number
<b>ETYPE</b>	Text (8)	Element Type. One of the following: <b>BAR</b> <b>QDMEM1</b> <b>QUAD4</b> <b>ROD</b> <b>SHEAR</b> <b>TRIA3</b> <b>TRMEM</b>
<b>EID</b>	Integer > 0	Element Identification Number

Created By: Module IFP

## 4. DISCUSSION OF RESULTS

### 4.1 Test Model

To verify the accuracy of the algorithm discussed in previous sections, a simple wing planform, shown in Figure 4-1, was selected. Figure 4-2 shows the smoothly deformable trailing edge control surface mechanism used in this analysis. A pair of solid state actuators were used to deform the trailing edge control surface. The actuators either pull or push the stringers. Thus, small amounts of bending moment are applied to the top and bottom skin surfaces so that the control surface can curl up or down according to the direction of the stimuli. In this model, ten actuators were used.

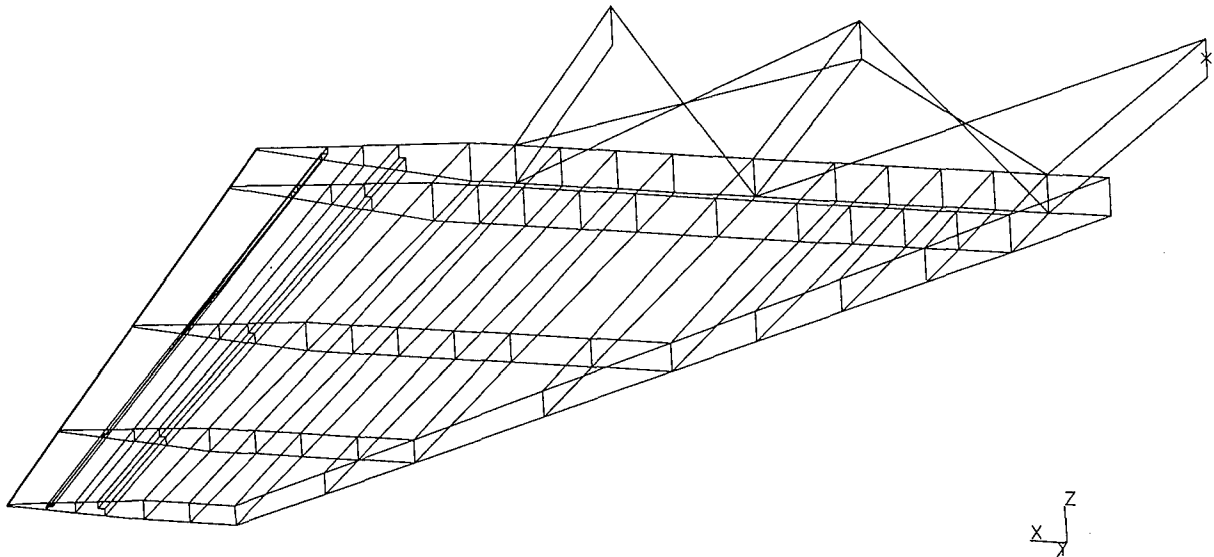


Figure 4-1. A low aspect ratio wing showing structural elements

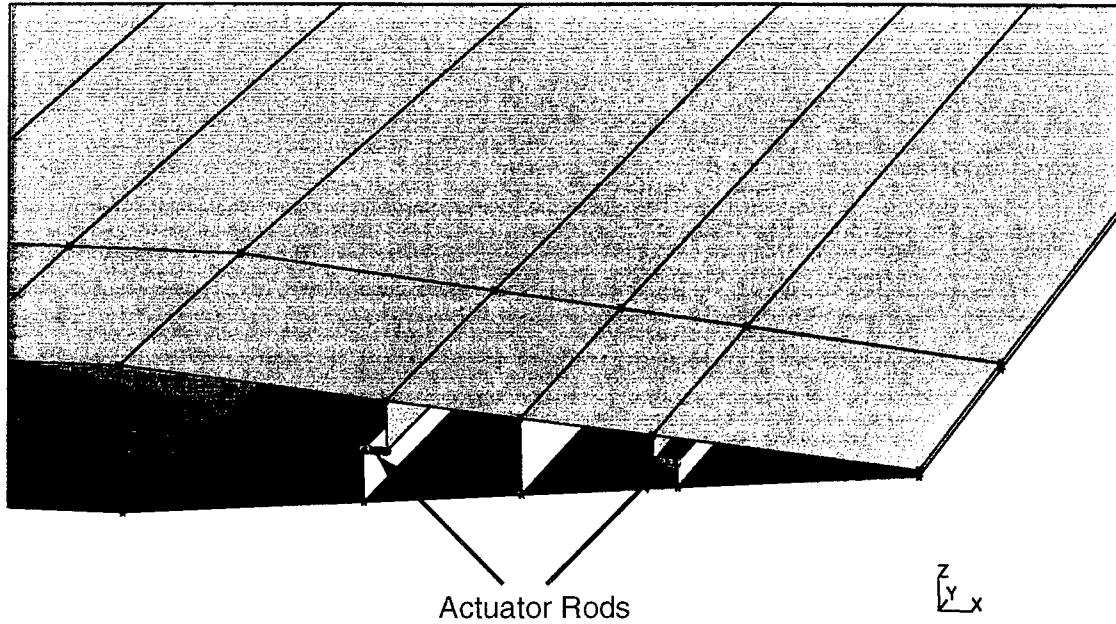


Figure 4-2. Trailing edge control surface showing solid state actuation mechanism

A number of performance analyses were conducted. The results are presented next.

#### 4.2 Test Case: Steady Roll Maneuver

Altitude	Sea level
Mach Number	$M = 0.5$
Roll rate	$p_T = 3.0$ radians/sec
Number of actuators	10 along wing trailing edge
Objective function	Minimum total power required
Constraints	Target value of $p_T$ , and strain allowable in the actuators

The deformed shape of the wing is shown in Figure 4-3.



The solid state actuators shown in Figure 4-2 are able to magnify their movement, also known as the mechanical advantage (MA), such as in the case of inchworm motors. This is necessary to accommodate large relative displacements between the end points or attachment points of the actuators. With this mechanism, relatively small forces will be able to provide necessary wing camber for desired maneuver performance. Table 4-1 through Table 4-3 show the effect of MA on actuator force requirements and consequently the total energy.

Mechanical	Advantage	1.00E+02		Net Energy = 1017. ft.lbs	
Actuator	Stimuli	Stress	Force	Energy	Displacement
Element	Volt	PSI	Lbs.	Inch.lbs	Inch
1	2.22E+01	-3.17E+04	-1.59E+03	4.00E+01	0.6
2	-2.22E+01	3.91E+04	1.96E+03	6.10E+01	0.28
3	1.52E+02	-2.84E+05	-1.42E+04	3.21E+03	0.495
4	-1.12E+02	2.17E+05	1.09E+04	1.88E+03	0.026
5	1.10E+02	-2.68E+05	-1.34E+04	2.87E+03	-0.431
6	-1.04E+02	2.49E+05	1.25E+04	2.47E+03	-1.494
7	44.19	-133566.6	-6678.3	711	-1.52
8	-36.21	110627.8	5531.3	488	-2.93
9	29.65	-83604.3	-4180.2	279.1	-2.28
10	-24.56	72489.1	3624.5	209.8	-3.74

**Table 4-1. Influence of Mechanical Advantage On Actuator Energy Requirement, MA = 100**

Mechanical	Advantage	5.00E+02		Net Energy = 309.00ft.lbs	
Actuator	Stimuli	Stress	Force	Energy	Displacement
Element	Volt	PSI	Lbs.	Inch.lbs	Inch
1	5.2	-10629.8	-531.5	4.5	0.598
2	-3.7	15760	788	9.89	0.28
3	31.17	-132418.1	-6620.9	698.2	0.489
4	-21.57	103784.2	5189.2	428.9	1.941
5	22.8	-158524.4	-7926.2	1002.2	-0.435
6	-19.9	143892.8	7194.64	825.7	-1.498
7	9.6	-90266	-4513.3	324.94	-1.514
8	-6.4	73313.2	3665.7	214.34	-2.921
9	6.7	-54929.37	-2746.5	120.5	-2.262
10	-4.096	46892.9	2344.64	87.79	-3.73

**Table 4-2. Influence of Mechanical Advantage On Actuator Energy Requirement, MA = 500**

Mechanical Advantage	Stimuli	Stress	Force	Energy	Displacement
Element	Volt	PSI	Lbs.	Inch.lbs	Inch
1	3.1	-8150.1	-407.5	2.65	0.59
2	-1.33	12911.8	645.6	6.64	0.27
3	16.03	-113551.6	-5677.6	513.4	0.48
4	-10.24	89644	4482.2	319.9	0.011
5	11.87	-144634.7	-7231.7	834.3	-0.44
6	-9.423	130595.9	6529.8	680.2	-1.5
7	5.29	-84770.3	-4238.5	286.6	-1.51
8	-2.7	68567.6	3428.4	187.5	-2.914
9	3.845	-51337.5	-2566.9	105.2	-2.24
10	-1.538	43671.5	2183.6	76.14	-3.71

**Table 4-3. Influence of Mechanical Advantage On Actuator Energy Requirement, MA = 1000**

Figure 4-7 shows the energy required to perform a 3.0 radian/second roll versus the mechanical advantage of an actuator. For MA less than 100, a large amount of input power is required to stretch the actuator to match the relative displacement between the end points of the actuator. Otherwise, desired roll rate cannot be achieved. For actuators with MA greater 400, the required energy is constant at 250 ft.lbs. This means the actuator is able to freely accommodate the expansion between the attachment points.

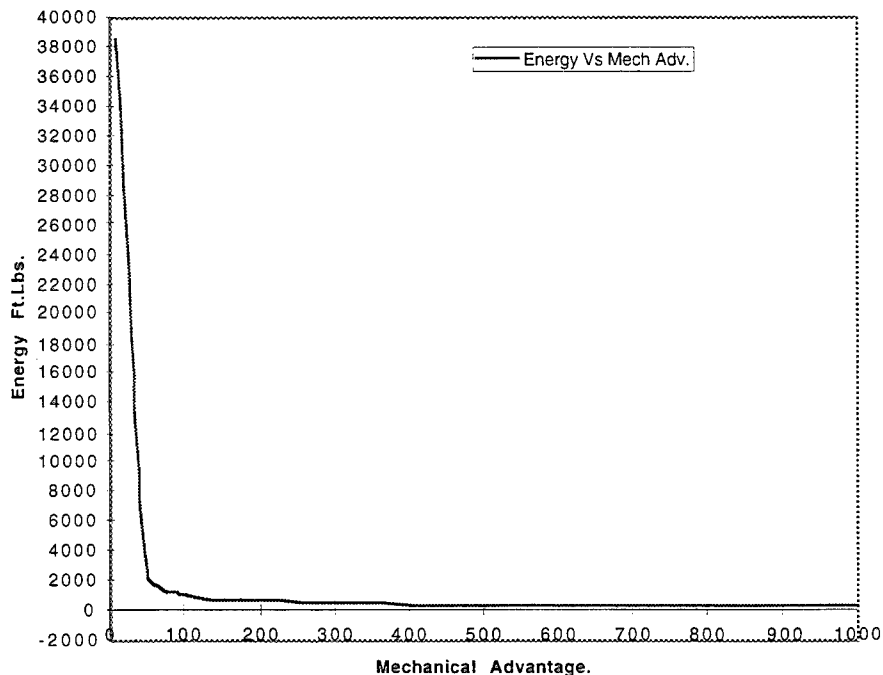


**Figure 4-7. Actuator Energy Vs. Mechanical Advantage.**

## 5. Conclusions and Recommendations

An analytical simulation algorithm based on optimal control theory has been developed to compute solid state actuator power and placement to achieve improved aircraft performance. This study suggests that the solid state actuators must be able to travel large distances between contact points so that the required power is minimized. The displacements between points can be on the order of half to one half inches. Such large displacements and large forces can be achieved by inchworm actuators.

The present study used a single degree of rigid body roll motion. Albeit, this algorithm can be extended to five degrees of freedom. Furthermore, modal degrees of freedom can be replaced by user-selected structural degrees of freedom.

## 6. REFERENCES

1. Wong, K. J., "AFTI/F-111 Mission Adaptive Wing Lift and Drag Flight Test Results," AFFTC-TR-87-02, Final Report, April 1987.
2. Hall, J. M., "Executive Summary AFTI/F-111 Mission Adaptive Wing," WRDC-TR-89-3083, September 1989.
3. Cogburn, L. T., "AFTI/F-111 Mission Adaptive Wing Flutter and Aeroservoelastic Test Program," AFFTC-TR-86-42, Final Report, March 1987.
4. Appa, K., Martin, C. A., Scherer, L. B., and Kudva, J. N.. "Aerodynamic Benefits of Hingeless Control Surfaces," SPIE Far East and Pacific Rim Symposium on Smart Materials and Structures, December, 11-14, 1996, Indian Institute of Science Bangalore, India.
5. Appa, K. "Recent Advances in Manoeuvre Loads Analysis," Computer Methods in Applied Mechanics and Engineering, Volume 90, Nos. 1-3, 1991, pp. 693-717.
6. Appa, K., and Argyris, J. "Computational Aircraft Dynamics and Loads," Sadhana, Vol. 19, Part 3, June 1994, pp. 467-485, Academy Proceedings in Engineering Sciences, Printed in India.
7. Appa, K., Argyris, J., Guruswamy, G. P., and Martin, C. A., "Synergistic Aircraft Design Using CFD Air Loads," AIAA-96-4057-CP, 6th AIAA/NASA/USAF Multidisciplinary Analysis & Optimization Symposium, September 4-6, 1996, Bellevue, WA.
8. Khot, N. S., Eastep, F. E., and Kolony, R. M., "Optimization of a Composite Wing Structure for Enhancement of the Rolling Maneuver," AIAA-96-3998-CP, 6th AIAA/NASA/USAF Multidisciplinary Analysis & Optimization Symposium, September 4-6, 1996, Bellevue, WA.